Three-dimensional computation of turbulent natural convection in the presence of magnetic field

JALAL M. JALIL*, TALIB K. MURTADHA AND KAYS A. AL-TAE'Y
University of Technology, Hay AL-Wahda, PO Box 35010, Baghdad, Iraq.
email: jalalmjalil@yahoo.com

Abstract

Numerical three-dimensional study is carried out on the turbulent natural convection of molten sodium (low Prandtl number fluid) in a cubic cavity heated from one vertical wall and cooled from an opposing vertical wall, with the other walls thermally insulated. The cavity is exposed to external uniform magnetic fields, either horizontal and perpendicular, to the heated wall (x-direction) or in vertical and parallel direction to the heated wall (y-direction) or in horizontal and parallel directions to the heated wall (z-direction). The magnetic field in the horizontal and perpendicular direction gave the smallest value of the average Nusselt number on the vertical heated wall and in the vertical and parallel direction the largest value. On the other hand, the external magnetic field in horizontal and parallel direction was found to be effective in between these two extremes. The effect of magnetic field on Nusselt number three-dimensional laminar flow is greater than that for two-dimensional laminar flow at same value of magnetic field intensity.

Keywords: Natural convection, turbulent flow, magnetic field, turbulent eddies.

1. Introduction

Natural convection is an important phenomena in crystal growth from the melt. A typical driving force for convection in the melt is the buoyancy force induced by thermal and solutal gradients in the liquid. Application of magnetic fields is to damp both flow and temperature oscillations in the melt and thereby represents a promising opportunity to obtain improved crystal quality [1].

The natural convection of an electrically conducting fluid in a cubic cavity in the presence of a magnetic field has been thoroughly studied by several researchers in the laminar flow $Ra \leq 10^6$ [1–5]. Comparatively little attention has been paid to the turbulent flow $Ra > 10^6$ which is also of interest for many industrial processes.

This paper is devoted to the study of turbulent convection heat transfer $Ra = 10^8$ in molten sodium under the influence of uniform magnetic field. The $(k–\varepsilon)$ turbulence model was used for $Ra = 10^8$. The effect of a magnetic field on average Nusselt number for $Ra = 10^6$ at two-dimensional flow has been compared with that at three-dimensional flow.

*Author for correspondence.
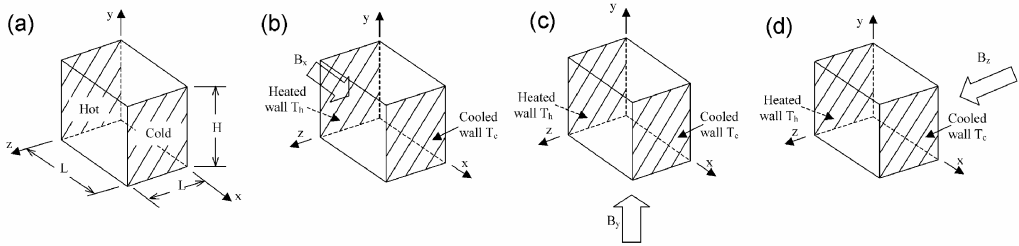
FIG. 1. (a) Schematic diagram of the enclosure and coordinate system: uniform magnetic field in (b) x-, (c) y-, (d) z-directions.

2. System considered

A schematic diagram of the physical situation to be investigated is shown in Fig. 1(a)–(d); the vertical walls of height H and depth Lz located at $x = 0$ and $x = L$ are isothermal at different temperatures of T_h and T_c ($T_h - T_c = 25°C$), respectively. Other four walls of width L are insulated at $y = 0$, $y = H$, $z = 0$ and $z = Lz$, and all six walls have electrically insulated boundaries. The molten sodium in the cubic cavity is exposed to external uniform magnetic fields, either horizontally and perpendicularly to the heated wall (x-direction), (Fig. 1(b)) or in a vertical direction (y-direction) (Fig. 1(c)) or in horizontal and parallel directions to the heated wall (z-direction) (Fig. 1(d)). The uniform magnetic field is generated with a C-type magnet. The cubic cavity is conducted in the framework of Boussinesq approximation, because $\beta (T - T_c) << 1$. Therefore, the fluid properties are assumed to be constant except the fluid density in its contribution to the buoyancy force in the momentum equation. The flow is treated as steady, and incompressible and is dependent on the Rayleigh number and Hartmann number.

3. Model equations and method of solution

The fluid in the cavity received both the buoyancy forces resulting from heat transfer through side walls and electromagnetic force resulting from convection of fluid in a uniform external magnetic field.

The flow in a cubic cavity is three dimensional, subject to a uniform magnetic field B_o of a constant magnitude B.

By Ohm's law without Hall effect and electrically insulated boundaries, the electric current density is

$$J = \sigma(E + V \times B) \tag{1}$$

and the electromagnetic force

$$F_{EM} = J \times B. \tag{2}$$

The induced magnetic field is small compared to the applied magnetic field ($Rm << 1$) so

$$B = B_O. \tag{3}$$

The electric field intensity is related to a scalar potential function (the gradient of the potential) by

$$E = -\nabla \psi_e. \tag{4}$$

From Kirchhoff's first law

$$\nabla \cdot J = 0. \tag{5}$$

Equations (1), (4) and (5) give the value of scalar potential function ψ_e

$$\nabla^2 \psi_e = \nabla \cdot (V \times B). \tag{6}$$

The flow is described by the continuity, momentum and energy equations as follows:

Continuity equation

$$\frac{\partial}{\partial x} \rho u + \frac{\partial}{\partial y} \rho v + \frac{\partial}{\partial z} \rho w = 0. \tag{7}$$

Momentum equations

x-direction momentum equation

$$\frac{\partial}{\partial x} \rho uu + \frac{\partial}{\partial y} \rho uv + \frac{\partial}{\partial z} \rho uw = \frac{\partial}{\partial x}\left(\mu \frac{\partial}{\partial x} \right) + \frac{\partial}{\partial y}\left(\mu \frac{\partial u}{\partial y} \right) + \frac{\partial}{\partial z}\left(\mu \frac{\partial u}{\partial z} \right) + S_u; \tag{8}$$

y-direction momentum equation

$$\frac{\partial}{\partial x} \rho uv + \frac{\partial}{\partial y} \rho vv + \frac{\partial}{\partial z} \rho vw = \frac{\partial}{\partial x}\left(\mu \frac{\partial v}{\partial x} \right) + \frac{\partial}{\partial y}\left(\mu \frac{\partial v}{\partial y} \right) + \frac{\partial}{\partial z}\left(\mu \frac{\partial v}{\partial z} \right) + S_v; \tag{9}$$

z-direction momentum equation

$$\frac{\partial}{\partial x} \rho uw + \frac{\partial}{\partial y} \rho vw + \frac{\partial}{\partial z} \rho ww = \frac{\partial}{\partial x}\left(\mu \frac{\partial w}{\partial x} \right) + \frac{\partial}{\partial y}\left(\mu \frac{\partial w}{\partial y} \right) + \frac{\partial}{\partial z}\left(\mu \frac{\partial w}{\partial z} \right) + S_w. \tag{10}$$

The radiation heat transfer and Joule heating are ignored, as also the viscous dissipation and pressure work terms, which are generally small; so, thermal energy equation becomes

$$\frac{\partial}{\partial x} \rho uT + \frac{\partial}{\partial y} \rho vT + \frac{\partial}{\partial z} \rho wT = \frac{\partial}{\partial x}\left(\Gamma \frac{\partial T}{\partial x} \right) + \frac{\partial}{\partial y}\left(\Gamma \frac{\partial T}{\partial y} \right) + \frac{\partial}{\partial z}\left(\Gamma \frac{\partial T}{\partial z} \right) + S_T. \tag{11}$$

For turbulence flow $Ra > 10^6$

$$S_u = -\frac{\partial P}{\partial x} + \frac{\partial}{\partial x}\left(\mu_{\text{eff}} \frac{\partial u}{\partial x} \right) + \frac{\partial}{\partial y}\left(\mu_{\text{eff}} \frac{\partial v}{\partial x} \right) + \frac{\partial}{\partial z}\left(\mu_{\text{eff}} \frac{\partial w}{\partial x} \right) + F_{EMx}. \tag{12}$$

$$S_v = -\frac{\partial P}{\partial y} + \frac{\partial}{\partial x}\left(\mu_{\text{eff}} \frac{\partial u}{\partial y} \right) + \frac{\partial}{\partial y}\left(\mu_{\text{eff}} \frac{\partial v}{\partial y} \right) + \frac{\partial}{\partial z}\left(\mu_{\text{eff}} \frac{\partial w}{\partial y} \right) + \rho g \beta (T - T_c) + F_{EMy}. \tag{13}$$

$$S_w = -\frac{\partial P}{\partial z} + \frac{\partial}{\partial x}\left(\mu_{\text{eff}}\frac{\partial u}{\partial z}\right) + \frac{\partial}{\partial y}\left(\mu_{\text{eff}}\frac{\partial v}{\partial z}\right) + \frac{\partial}{\partial z}\left(\mu_{\text{eff}}\frac{\partial w}{\partial z}\right) + F_{EMz}. \tag{14}$$

$$S_T = 0.0. \tag{15}$$

$$\mu_{\text{eff}} = \mu + \mu_t. \tag{16}$$

$$\Gamma = \Gamma_{\text{eff}} = \frac{\mu}{\text{Pr}} + \frac{\mu_t}{\text{Pr}_t}. \tag{17}$$

For turbulent flows, the value of μ in eqns (8)–(10) is equal to μ_{eff}. It is known that in the presence of a sufficiently strong magnetic field the turbulent fluctuations become anisotropic, which implies strong effect on turbulence requiring probable modifications to numerical models. Specific manifestation of the anisotropy may vary but the principle mechanism is always the elongation of flow structures (turbulent eddies) along the lines of the magnetic field.

From the previous situation, the appropriate method to find the value of turbulent dynamic viscosity μ_t is by the use DNS or LES method. These methods require the solution region made fine enough to encompass the smallest eddy scale (eddy Reynolds number is unity) and at the same time large enough to include the largest eddies. But this needs sufficient number of grid points; these are unavailable in computer CPU 1.7 A. Another method which can be followed to find the value of μ_t is the use of k–ε model of turbulence. This model must be modified to include magnetic field effect.

The turbulent kinetic energy equation, k, and the dissipation rate of turbulent kinetic energy equation, ε, have not been modified due to the combination of electromagnetic and buoyancy force effect, as the turbulent structure intensity is low due to low Rayleigh number value used in this study, $Ra = 10^8$.

The turbulent viscosity μ_t in eqn (16) was determined from

$$\mu_t = C_\mu \rho \frac{k^2}{\varepsilon}. \tag{18}$$

The $(k - \varepsilon)$ model takes the following forms of three-dimensional steady flow [6]:

Turbulence energy, k

$$\frac{\partial}{\partial x}\rho u k + \frac{\partial}{\partial y}\rho v k + \frac{\partial}{\partial z}\rho w k = \frac{\partial}{\partial x}\left(\Gamma_k\frac{\partial k}{\partial x}\right) + \frac{\partial}{\partial y}\left(\Gamma_k\frac{\partial k}{\partial y}\right) + \frac{\partial}{\partial z}\left(\Gamma_k\frac{\partial k}{\partial x}\right) + G_s - C_D\rho\varepsilon \tag{19}$$

Dissipation rate, ε

$$\frac{\partial}{\partial x}\rho u\varepsilon + \frac{\partial}{\partial y}\rho v\varepsilon + \frac{\partial}{\partial z}\rho w\varepsilon = \frac{\partial}{\partial x}\left(\Gamma_\varepsilon\frac{\partial \varepsilon}{\partial x}\right) + \frac{\partial}{\partial y}\left(\Gamma_\varepsilon\frac{\partial \varepsilon}{\partial y}\right) + \frac{\partial}{\partial z}\left(\Gamma_\varepsilon\frac{\partial \varepsilon}{\partial z}\right) + C_1\frac{\varepsilon}{k}G_s - C_2\rho\frac{\varepsilon^2}{k} \tag{20}$$

where

$$\Gamma_k = \frac{\mu_{\text{eff}}}{\text{Pr}_k};$$ (21)

$$\Gamma_\varepsilon = \frac{\mu_{\text{eff}}}{\text{Pr}_\varepsilon};$$ (22)

$$G_s = \mu_t \left\{ 2 \left[\left(\frac{\partial u}{\partial x}\right)^2 + \left(\frac{\partial v}{\partial y}\right)^2 + \left(\frac{\partial w}{\partial z}\right)^2 \right] + \left(\frac{\partial u}{\partial y} + \frac{\partial v}{\partial x}\right)^2 + \left(\frac{\partial u}{\partial z} + \frac{\partial w}{\partial x}\right)^2 + \left(\frac{\partial v}{\partial z} + \frac{\partial w}{\partial y}\right)^2 \right\}.$$ (23)

Equation (2) gives the value of electromagnetic force in eqns (12)–(14) as follows: The electromagnetic force in x-direction uniform magnetic field, Fig. 1(b), is:

$$F_{EMy} = \sigma(E_z B_x - v B_x^2) \, j.$$ (24)

The electromagnetic force of y-direction uniform magnetic field, Fig. 1(c), is:

$$F_{EMx} = \sigma(-E_z B_y - u B_y^2) i.$$ (25)

The electromagnetic force of z-direction uniform magnetic field, Fig. 1(d), is:

$$F_{EMy} = \sigma(-E_x B_z - v B_z^2) \, j.$$ (26)

The ensemble average of the fluctuation electromagnetic force in the momentum equation was neglected. The value of w-velocity component is very small compared with that of u- and v-velocity components, hence the electromagnetic force, F_{EMz} in z-momentum, eqn (14), is neglected.

For turbulent flow at $Ra > 10^6$ and in the region near the solid surfaces the gradient of flow property variation is high, the local Reynolds number (y^+ or x^+) is extremely small and the turbulent viscosity is no longer dominant. The $(k - \varepsilon)$ model is not valid in this region and a special treatment is required to describe the flow properties. The wall function method is used to deal with this problem. The wall functions are based on one-dimensional steady-state boundary layer equations and mixing-length hypothesis. The principle of the method is to modify the source term in the conservation equations for the grid nodes near the solid surfaces by using the momentum flux due to shear stress and the heat flux at solid surface.

4. Computed results and discussion

4.1. *Code validation*

An important step in code development is to validate and compare the results computed from the code developed with published data from other computational codes.

The results at $Ra = 10^8$ computed by code development for two-dimensional flow of air filed square enclosure are shown in Fig. 2. The stream functions and isotherms are in good agreement with the results of Markatose and Pericleous [7].

Table I
Effect of grid number on the average Nusselt number value at *Ra* 10^8 and *Ha* = 0.0

x, y, z	$\overline{Nu}$
$51 \times 51 \times 21$	31.74
$61 \times 51 \times 21$	33.23
$61 \times 61 \times 21$	28.47
$61 \times 61 \times 43$	28.76
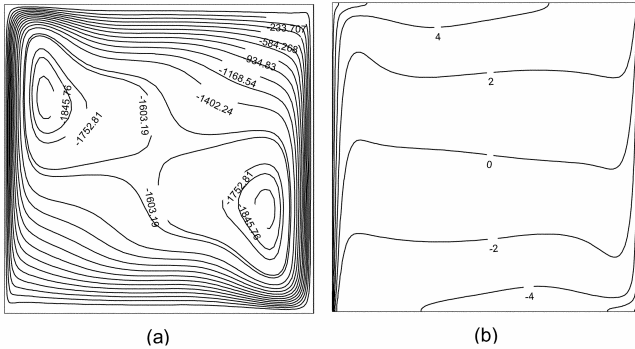
FIG. 2. For two-dimensional flow at $Ra = 10^8$, $Pr = 0.71$ and $Ha = 0.0$: (a) stream functions (mm²/s); and (b) isotherms (°C).

The conservation equation of mass, momentum and energy are solved by Patankar's [8] SIMPLE algorithm with hybrid difference scheme.

Constraints on the computing equipment (CPU 1.7A) have limited the use of small mesh intervals for higher accuracy. Calculations were made to determine the optimum mesh (Table I). The Nusselt number values varied with the number of mesh points, but not much beyond $61 \times 61 \times 21$. So the nonuniform grid was employed using $(x, y, z) = 61 \times 61 \times 21$ mesh in most of the calculations. The location of the first grid point near the walls used is $(\Delta x)_{min} = 0.4$ mm, $(\Delta y)_{min} = 0.4$ mm and $(\Delta z)_{min} = 1.33$ mm.

4.2. *Turbulent natural-convection heat transfer of a liquid metal without the effect of a magnetic field*

For turbulent flow at $Ra = 10^8$ and without magnetic field effect, $Ha = 0$, the velocity vectors and isotherms are represented in Fig. 3. The arrows denote the direction and magnitude of the resolved u-, v- and w-velocity components at each grid point in the flow region. The flow of molten sodium in the boundary layer regime is so strong that hot fluid has been carried over to the cooler side of the cavity, and vice versa. The w-velocity values are very small compared with those of u and v but are not zero.
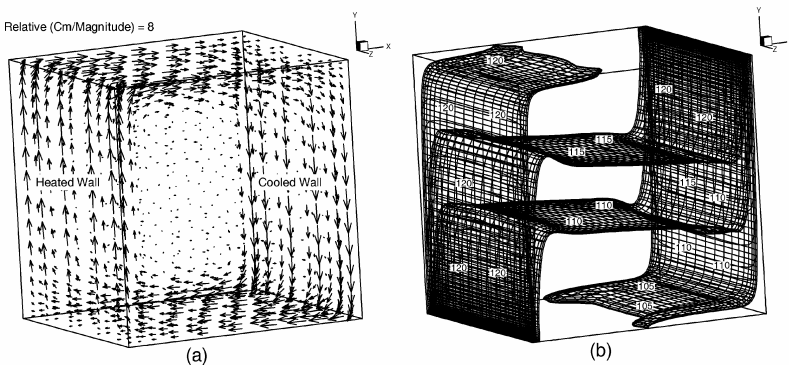
FIG. 3. At $Ra = 10^8$ and $Ha = 0$: (a) velocity vectors (m/s), and (b) isotherms (°C).
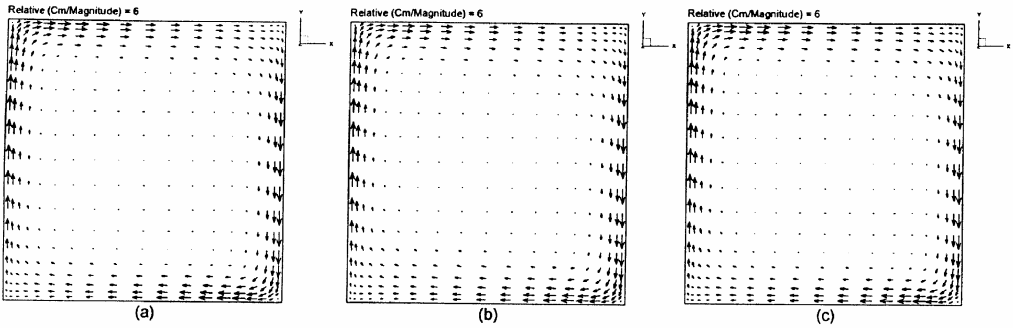
FIG. 4. Velocity vectors (m/s) in the x–y plane at $Ra = 10^8$ and $Ha = 0$; at z = (a) ¼, (b) ½, and (c) ¾ Lz.

The temperature is constant on horizontal lines in the layer of the central part. The temperature gradients are concentrated in two layers adjacent to the heated and the cooled walls, and the distortion of the temperature field near the corners, however, can be attributed to convective energy transport. This behavior of the temperature field can be interpreted as two thermal boundary layers on both vertical surfaces separated by a core with a temperature which is constant along horizontal lines but not along vertical lines.

The velocity vectors in vertical plane x–y are represented in Fig. 4 at three different levels of cavity depth, at quarter, mid and third planes. The velocity vectors of Fig. 4 indicate that the recirculation flow is adjacent to the walls, the central core of fluid is practically stagnant and the velocity maximum value moves closer to the wall as the Rayleigh numbers increase. Small change occurs in velocity values and flow patterns at x–y plane for the three different levels. This may be due to the effect of w-velocity, which is small.

The velocity vectors in the horizontal plane x–z are represented in Fig. 5. One can show that the w-velocity values are very small compared to those of u and v especially at y = ¼ and ¾ H.

For turbulent flow at y = ½ H (Fig. 5(b)), four weak eddies are formed and clearly the flow is not two-dimensional at this plane. On horizontal planes above and below the plane y = ½ H, the transversal base flow predominates over these weak eddies. Lankhorst *et al*.
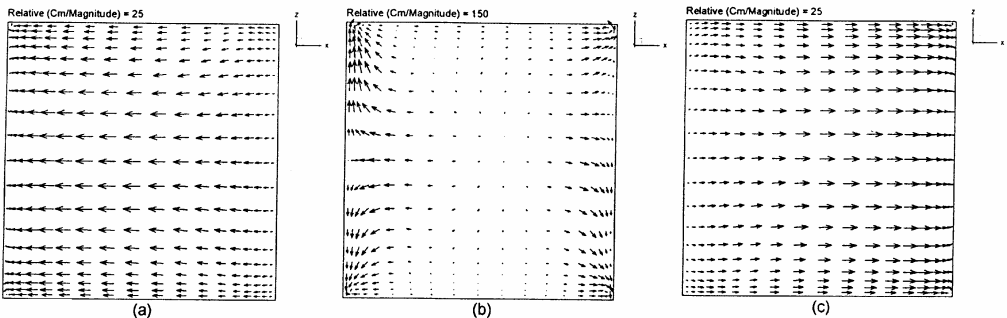
Fig. 5. Velocity vectors (m/s) in the x–z plane at $Ra = 10^8$ and $Ha = 0$: at y = (a) ¼, (b) ½, and (c) ¾ H.
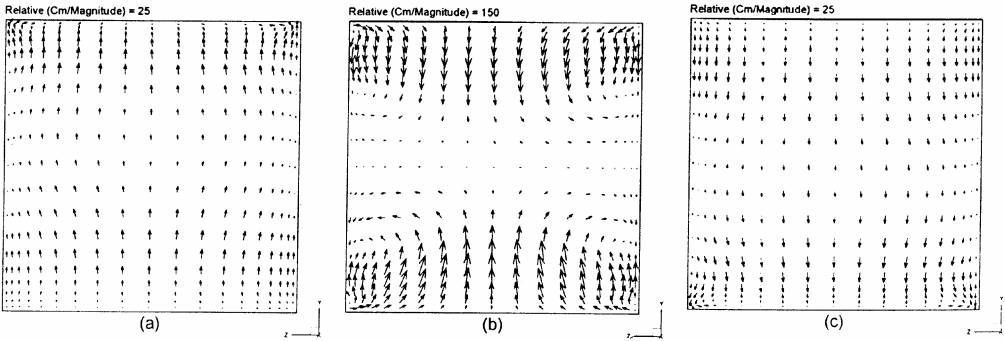
Fig. 6. Velocity vectors (m/s) in the y–z plane at $Ra = 10^8$ and $Ha = 0$: at x = (a) ¼, (b) ½, and (c) ¾ L.

[9] find that near the end walls the fluid moves more slowly and the convective heat transfer from the isothermal walls to the fluid is reduced. This creates a non-zero temperature gradient in z-direction.

The velocity vectors in vertical plane y–z are represented in Fig. 6. At x = ½ L, the weak effect of the w-velocity occurs at the corners of cavity and the flow is ascending and descending from the lower and upper parts of the cavity, respectively, and moves towards the core region. Hence the flow is not two dimensional at this plane (Fig. 6(b)). The temperature distribution contours show that the isotherms are denser on the lower part of the heated vertical wall and the top part of the cooled wall.

4.3. *Effect of direction of external uniform magnetic field on natural convection in enclosed cavity*

This section discusses the results of the effect of uniform magnetic field on the natural convection of molten sodium at a certain value of Rayleigh number (10^8) and different values of Hartmann number, the range being 0.00225–0.2 Tesla.

For turbulent flow at $Ra = 10^8$ and at $Ha = 1211$ and 4844, the velocity vectors and isotherms for x-, y-, and z-direction magnetic fields are represented in Figs 7–12, respectively.
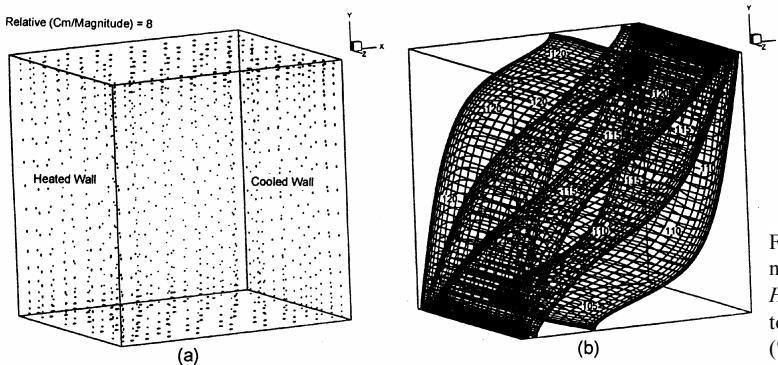
FIG. 7. At x-direction magnetic field for $Ra = 10^8$ and $Ha = 1211$: (a) velocity vectors (m/s); and (b) isotherms (°C).
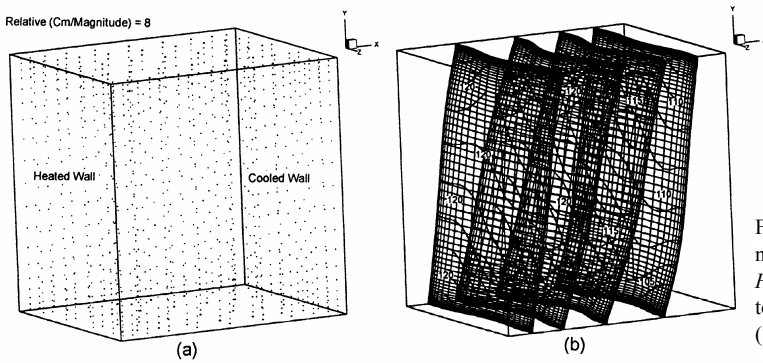
FIG. 8. At x-direction magnetic field for $Ra = 10^8$ and $Ha = 4844$: (a) velocity vectors (m/s); and (b) isotherms (°C).

The value of velocity vectors decreases with increase in magnetic field strength or Hartmann number from that at zero. The isotherms tend to become parallel to the vertical heated and cooled walls at high value of Hartmann number so convection decreases and most of the heat transfer is by heat conduction. For turbulent flow at $Ha = 1211$ the x-and z-direction magnetic fields have greater effect on velocity vectors and temperature distribution, and the y-direction has less effect (Figs 7, 9 and 11). At $Ha = 4844$, a small difference appears between the effects of x-, y- and z-direction magnetic fields on flow pattern. This is due to high reduction in the flow strength by the electromagnetic force effect at this value of Hartmann number (Figs 8, 10, 12).

The velocity vectors in the vertical x–y plane for x- and y-direction magnetic field are illustrated in Figs 13 and 14, respectively, at three different levels of cavity depth. The velocity vectors in x–y plane are u-velocity parallel to x-axis, and v- to y-axis. The x-direction magnetic field has direct and indirect effect on v- on u-velocity vectors, respectively, by continuity equation. Hence, the u-velocity vectors adjacent to the upper and lower adiabatic walls are greater than the v vectors adjacent to the heated and cooled walls (Fig. 13). But the y-direction magnetic field has direct and indirect effect on u- and v-velocity vectors, respectively, by continuity equation. Hence, the *v*-velocity vector adjacent to the heated and cooled walls is greater than the u-velocity vectors adjacent to the upper and lower adiabatic
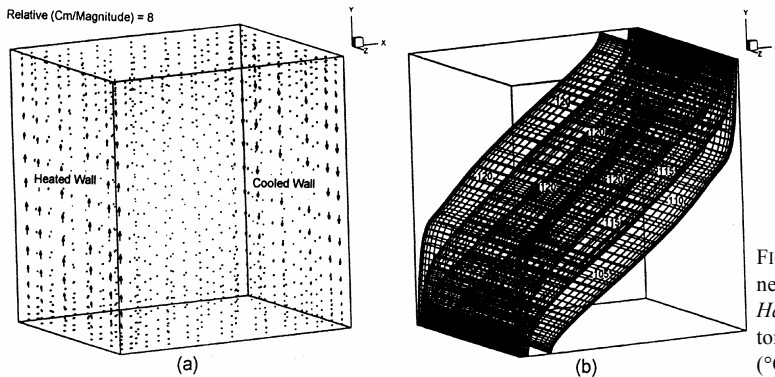
FIG. 9. At y-direction magnetic field for $Ra = 10^8$ and $Ha = 1211$: (a) velocity vectors (m/s); and (b) isotherms (°C).
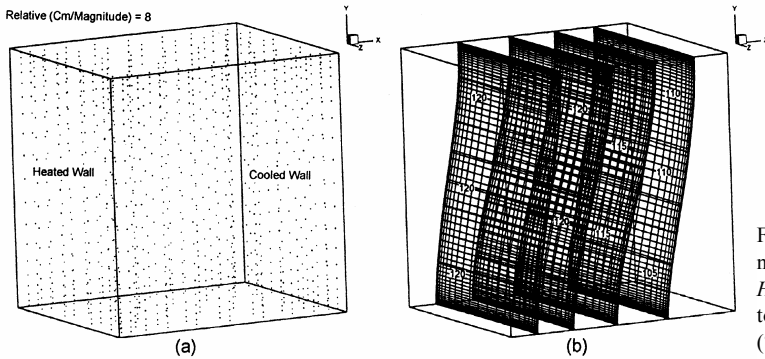
FIG. 10. At y-direction magnetic field for $Ra = 10^8$ and $Ha = 4844$: (a) velocity vectors (m/s); and (b) isotherms (°C).

walls (Fig. 14). Then the x- and y-direction magnetic fields have effect on flow pattern of molten sodium and temperature distribution. The flow pattern and temperature distribution at the z-direction magnetic field has similar effect by of x-direction magnetic field effect.

For $Ha = 1211$, the flow patterns change from that at $Ha = 0$. This is due to the effect of the electromagnetic force on u-, v- and w-velocity vectors. The two secondary vortices appear adjacent to the heated and the cooled walls at the y-direction magnetic field (Fig. 14). This is due to the high suppression of the flow at the upper and lower adiabatic walls caused by electromagnetic force appearing in x-momentum equation. In general, to generate two secondary vortices at the heated and cooled walls, the u-velocity values for the fluid adjacent to the upper and lower walls must decrease to the values to make the ascending and descending flow change direction and generate vortex. The v-velocity value is larger than the u-velocity value. So the values of electromagnetic force needed to damp the v-velocity are greater than those needed to damp the u-velocity.

The horizontal x–z plane for velocity vectors at the x- and y-direction magnetic field are illustrated in Figs 15 and 16, respectively. For x-direction magnetic field, and at y = ¼ H or near the lower adiabatic wall as in Fig. 15(a), two secondary vortices appear at the lower corners of the heated wall. When y = ½ H, the four weak eddies that appear at $Ha = 0$, as in
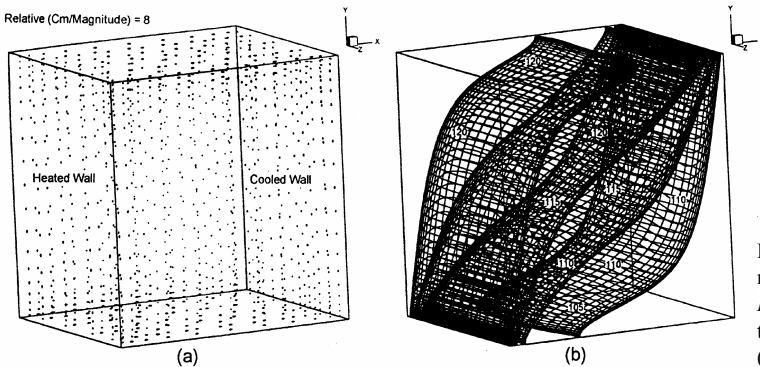
FIG. 11. At z-direction magnetic field for $Ra = 10^8$ and $Ha = 1211$: (a) velocity vectors (m/s); and (b) isotherms (°C).
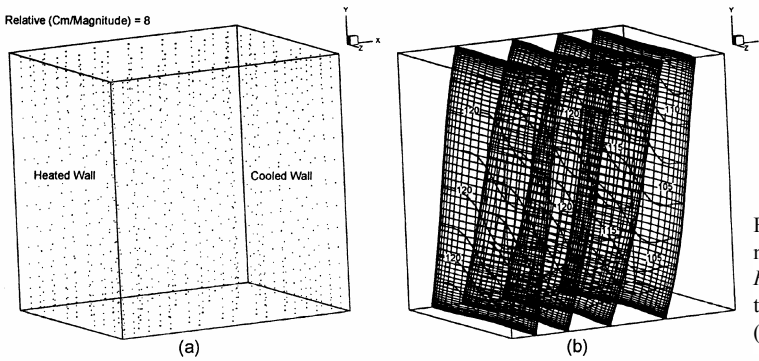
FIG. 12. At z-direction magnetic field for $Ra = 10^8$ and $Ha = 4844$: (a) velocity vectors (m/s); and (b) isotherms (°C).

Fig. 5(b), grow and move closer towards the centre of cavity (Fig. 15(b)). For y-direction magnetic field no eddies appear in the horizontal x–z plane at y = ¼ H and y = ¾ H (Fig. 16(a) and (c)). The pattern of flow at y = ½ H is as shown in Fig. 16(b). This is due to the two secondary vortices which appear in x–y plane (Fig. 14(b)).

The vertical y–z plane for velocity vectors at the x- and y-direction magnetic field are illustrated in Figs 17 and 18, respectively, for $Ra = 10^8$ and $Ha = 1211$. For x-direction magnetic field and at x = ½ L as in Fig. 17(b), very weak effect of w-velocity occurs at the corners of cavity but in opposite direction to that which happens at $Ha = 0$ as in Fig. 6(b). For y-direction magnetic field and at x = ¼ and ¾ L the molten sodium is descending and ascending along the heated and cooled wall as shown in Fig. 18(a) and (c), respectively. This is due to the two secondary vortices, which appear in the x–y plane as shown in Fig. 14, and the two secondary vortices appear at the upper and lower corners when x = ¼ and ¾ L.

The turbulent kinetic energy (k) distribution at x-direction magnetic field is shown in Fig. 19. It decreases due to increase in magnetic field strength, affects fluctuation velocity and decays MHD turbulence. This effect on eddy viscosity values and distribution is shown in Fig. 20.
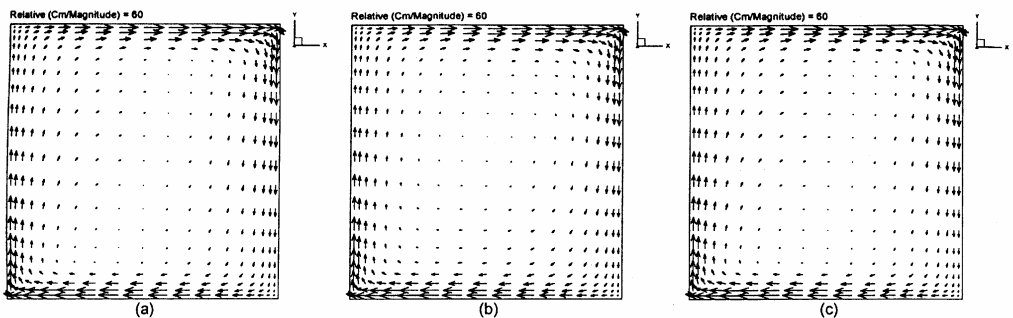
FIG. 13. Velocity vectors (m/s) in the x–y plane at x-direction magnetic field for $Ra = 10^8$ and $Ha = 1211$: at z = (a) ¼, (b) ½, and (c) ¾ Lz.
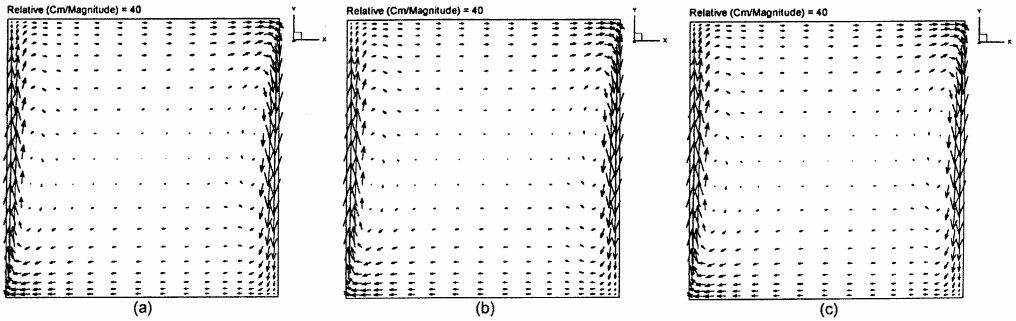
FIG. 14. Velocity vectors (m/s) in the x–y plane at y-direction magnetic field for $Ra = 10^8$ and $Ha = 1211$: at z = (a) ¼, (b) ½, and (c) ¾ Lz.

The average Nusselt number value for $Ra = 10^8$ at $Ha = 0.0$ (without magnetic field effect) is $\overline{Nu} = 28.47$. The same at different values of Hartmann number are shown in Table II. In general, the average Nusselt numbers decrease with increase in Hartmann number.

The average Nusselt number values are slightly different from each other under this magnetic field effect. However, the difference is apparent. The magnetic field in the x-direction gives the smallest value of average Nusselt numbers on the vertical heated wall. In y-direction it gives the largest value and in z-direction is found to be effective in between these two extremes. The effect of the electric field intensity E that appears in the electro-magnetic force equations is damping or reinforces the electromagnetic force strength.

The values of average Nusselt number for laminar flow at $Ra = 10^6$ and for three-dimensional flow are compared with that for the two-dimensional flow (neglecting the effect of z-direction) by using the following expression of free convection efficiency term [10], C_{effici}:

$$C_{effici}\ \frac{\overline{Nu_B}}{\overline{Nu_B} + \overline{Nu_{B=0}}}, \tag{27}$$
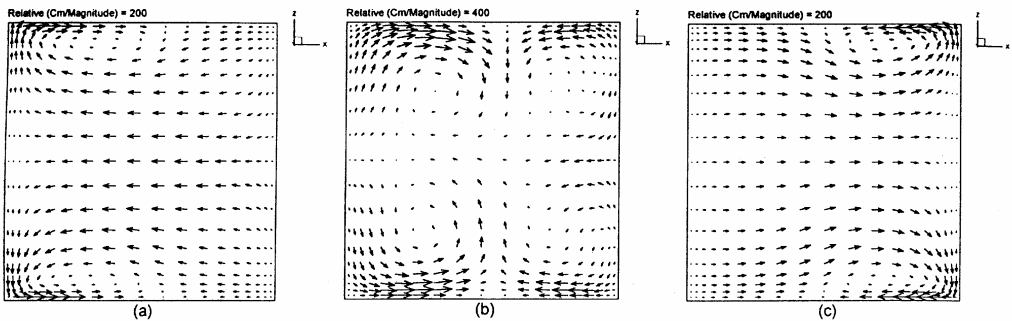
FIG. 15. Velocity vectors (m/s) in the x–z plane at x-direction magnetic field for $Ra = 10^8$ and $Ha = 1211$: at y = (a) ¼, (b) ½, and (c) ¾ H.
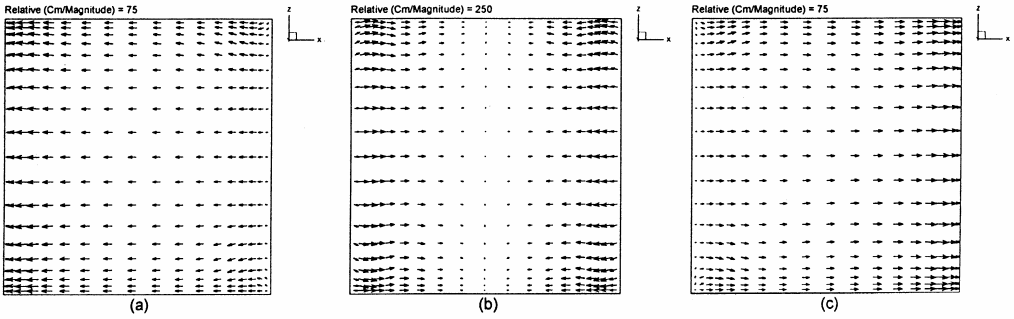
FIG. 16. Velocity vectors (m/s) in the x–z plane at y-direction magnetic field for $Ra = 10^8$ and $Ha = 1211$: at y = (a) ¼, (b) ½, and (c) ¾ H.

where C_{effici} is Efficiency of convection, $\overline{Nu}_{B=0}$, the average Nusselt number without external uniform magnetic field or at $Ha = 0$, and $\overline{Nu}_B$, the average Nusselt number with external uniform magnetic field or at $Ha \neq 0$.

The results for x- and y-direction magnetic fields are shown in Table III. The effect of magnetic field on the three-dimensional flow is found to be greater than on the two-dimensional flow. The difference in average Nusselt number values between three- and two-dimensional flow increases with increase in Hartmann number values. For example, at $Ha = 78.27$ and for x-direction magnetic field, the difference in value of C_{effici} between three- and two-dimensional flow is 0.695, but at high value of $Ha = 521.8$ it is 2.816.

The results of average Nusselt number values in this investigation are not in agreement with those of Ozoe and Okada [2] for the nature of effect of z- and y-direction magnetic fields. They studied the effect of x-, y- and z-direction uniform magnetic fields on laminar natural convection of molten silicon in an enclosed cavity. They found the horizontal and perpendicular direction to the heated wall magnetic field (x-direction) to be most effective in suppression of the convection and has the least value of average Nusselt number. But the horizontal and parallel direction to the heated wall magnetic field (z-direction) is less effect-
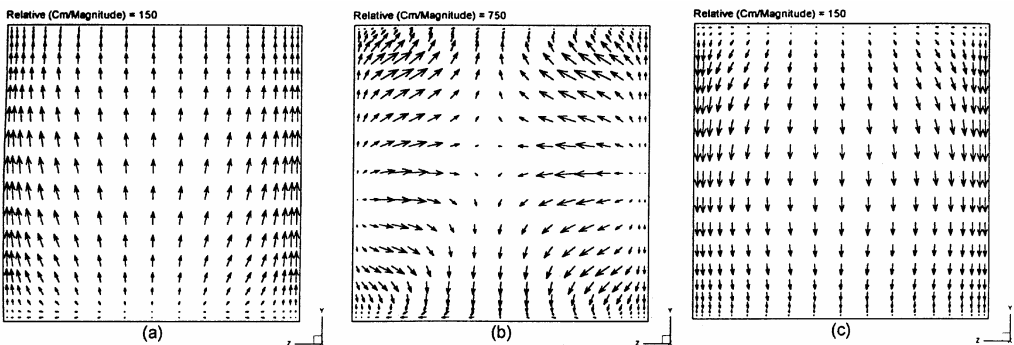
FIG. 17. Velocity vectors (m/s) in the y–z plane at x-direction magnetic field for $Ra = 10^8$ and $Ha = 1211$: at x = (a) ¼, (b) ½, and (c) ¾ L.

Table II
Effect of Hartmann number on an average Nusselt number at turbulent flow ($Ra = 10^8$) for uniform magnetic field

Ha	$\overline{Nu}$		
	B_x	B_y	B_z
54.5	28.33	28.48	28.34
84.77	28.13	28.46	28.15
181.7	26.84	28.16	26.91
545	17.44	23.96	17.57
1211	8.575	13.33	8.620
2422	3.917	4.364	3.928
4844	2.552	2.480	2.536

Table III
The efficiency of free convection C_{effici} at x- and y-direction magnetic fields for two- and three-dimension flow at laminar flow $Ra = 10^6$

Ha	C_{effici} (%) at B_x		C_{effici} (%) at B_y	
	Two-dimensional	Three-dimensional	Two-dimensional	Three-dimensional
52.18	46.338	45.769	46.27	45.841
78.27	42.425	41.73	43.005	42.49
130.4	34.689	32.992	37.162	36.18
260.9	23.062	20.279	23.678	21.459
391.3	19.166	16.319	19.07	16.38
521.8	18.024	15.208	17.947	15.15
1044	17.39	14.56	17.39	14.63

tive in suppression of the convection and has a high value of average Nusselt number at the same Hartmann number value. And, the vertical and parallel direction to the heated wall magnetic field (y-direction) was found to be effective between these two extremes.

An experimental study by Okada and Ozoe [3] shows that the z-direction magnetic field causes enhancement in heat-transfer rate of laminar natural convection for $Pr = 0.024$ (mol-
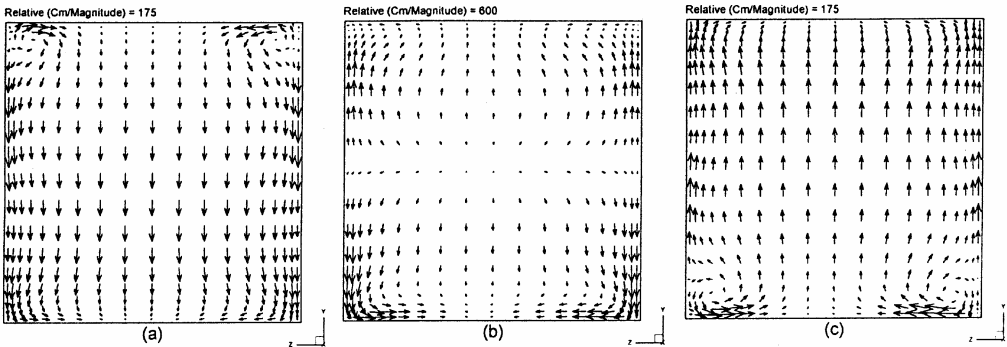
FIG. 18. Velocity vectors (m/s) in the y–z plane at y-direction magnetic field for $Ra = 10^8$ and $Ha = 1211$: at x = (a) ¼, (b) ½, and (c) ¾ L.
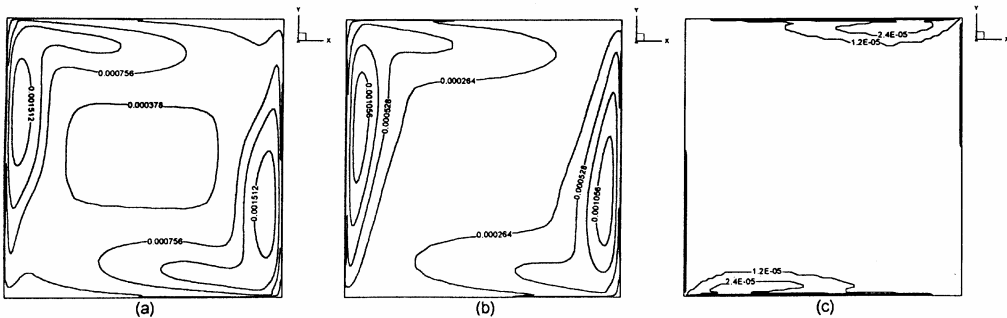
FIG. 19. Turbulence kinetic energy (m²/s²) for $Ra = 10^8$ and at x-direction magnetic field B_x in the x–y plane at z = ½ Lz: *Ha* (a) 0.0, (b) 181.7, and (c) 2422.

FIG. 20. Turbulent viscosity of fluid (kg/ms) for $Ra = 10^8$ and at x-direction magnetic field B_x in the x–y plane at $z = \frac{1}{2} Lz$: Ha (a) 0.0, (b) 181.7, and (c) 2422.

ten gallium) and at low Hartmann number values. Another study by Tagawa and Ozoe [4] shows that the heat transfer rate for z-direction magnetic field enhances for molten gallium at low Hartmann number. But, in our investigation, enhancement did not appear in heat-transfer rate due to the magnetic field application; so this result agrees with the numerical study of Ozoe and Okada [2]. They did not find any enhancement in laminar heat transfer rate for z-direction magnetic field.

5. Conclusion

A numerical study was carried out for the effect of x-, y- and z-direction uniform magnetic field on three-dimensional flow and temperature distribution of molten sodium turbulent natural convection in an enclosed cavity heated from one vertical wall and cooled from an opposing vertical wall. The results show that the x-direction external magnetic field was found to be the most effective in suppressing convection, and the y-direction field to be the least effective. The external z-direction magnetic field was found to be effective in between these two extremes, e.g. at $Ha = 545$ the reduction in Nusselt number value at B_x is 38.74%, B_y 15.84% and B_z 38.28%.

The average Nusselt number values decrease with increase in Hartmann number values. For laminar flow at $Ra = 10^6$, the effect of magnetic field in three-dimension flow on heat transfer coefficient was found to be greater than in two-dimensional flow.

The present numerical study would be useful to study two-phase flow and heat transfer when the turbulent flow is generated due to flow of gas bubble through liquid metal and with effect of a magnetic field.

References

1. G. M. Oreper, and J. Szekely, The effect of an externally imposed magnetic field on buoyancy driven flow in a rectangular cavity, *J. Crystal Growth*, **64**, 505–515 (1983).

2. H. Ozoe, and K. Okada, The effect of the direction of the external magnetic field on the three-dimensional natural convection in a cubical enclosure, *Int. J. Heat Mass Transfer*, **32**, 1939–1954 (1989).

3. K. Okada, and H. Ozoe, Experimental heat transfer rates of natural convection of molten gallium suppressed under an external magnetic field in either the X-, Y- or Z-direction, *J. Heat Transfer*, **114**, 107–114 (1992).

4. T. Tagawa, and H. Ozoe, Enhanced heat transfer rate measured for natural convection in liquid gallium in a cubical enclosure under a static magnetic field, *ASME J. Heat Transfer*, **120**, 1027–1032 (1998).

5. R. Sampath, and N. Zabaras, Numerical study of convection in the direction solidification of a binary alloy driven by the combined action of buoyancy, surface tension, and electromagnetic forces, *J. Comput. Phys.*, **168**, 384–411 (2001).

6. J. M. Jalil, T. K. Murtadha, and K. A., Al-Tae'y, Laminar and turbulent natural convection heat transfer of a liquid metal in an enclosed cavity, to be published in *Engineering Journal of the University of Qatar*.

7. N. C. Markatos, and K. A. Pericleous, Laminar and turbulent natural convection in an enclosed cavity, *Int. J. Heat Mass Transfer*, **27**, 755–772 (1984).

8. S. V. Patankar, *Numerical heat transfer and fluid flow*, Hemisphere (1980).

9. A. M. Lankhorst, R A W. M. Henkes, and C. J. Hoogendoorn, Natural convection in cavities at high Rayleigh number, computations and validation, *Second UK National Conf. on Heat Transfer*, University of Strathclyde, Glasgow, September 14–16, 1988, Vol. 1, pp. 353–370.

10. M. F. Haque, and S. Arajs, Convective heat transfer in fluids in the presence of gravitational and electro-magnetic fields, *Il Nuovo Cimento D*, **19**, 665–684 (1997).

Nomenclature

B	Magnetic induction (Tesla)
B_x	Magnetic induction in x-direction (Tesla)
B_y	Magnetic induction in y-direction (Tesla)
B_z	Magnetic induction in z-direction (Tesla)
B_o	External magnetic field (Tesla)
C_1, C_2, C_D, C_μ	Coefficients in turbulence model
E	Electric field intensity (volt/m)
F_{EM}	Electromagnetic force (N/m^3)
F_{EMx}	Electromagnetic force in x-direction (N/m^3)
F_{EMy}	Electromagnetic force in y-direction (N/m^3)
F_{EMz}	Electromagnetic force in z-direction (N/m^3)
g	Acceleration due to gravity (m/s^2)
H	Enclosure height (m)
Ha	Hartmann number
i, j, k	Unit vectors in x-, y-, z-directions, respectively
J	Electric current density (A/m^2)
k	Turbulence kinetic energy (m^2/s^2)
L	Enclosure width (m)
L_z	Enclosure depth (m)
$\overline{Nu}$	Average Nusselt number
P	Pressure (N/m^2)
Pr	Prandtl number
Ra	Rayleigh number
Rm	Magnetic Reynolds number
T	Temperature (K)
T_c	Cold wall temperature (K)
T_h	Hot wall temperature (K)

u	Velocity of x-component (m/s)
V	Velocity vector (m/s)
v	Velocity of y-component (m/s)
w	Velocity of z-component (m/s)
x, y, z	Cartesian coordinate (m)

Greek letters

β	Volumetric coefficient of expansion (K^{-1})
μ	Dynamic viscosity of fluid (kg/ms)
ρ	Density of fluid (kg/m^3)
σ	Electric specific conductivity of fluid (S/m)
ψ_e	Scalar potential function (volt)
ε	Dissipation energy rate (m^2/s^3)

Subscripts

eff	Effective
t	Turbulence